



Modeling reactive ammonia uptake by secondary organic aerosol in CMAQ: application to the continental US

Shupeng Zhu, Jeremy R. Horne¹, Julia Montoya-Aguilera²,
Mallory L. Hinks², Sergey A. Nizkorodov², and Donald Dabdub

Xie Feng
2018/10/4



Outline

- Introduction
- Methods
- Results
- Discussion



Introduction

Abstract:

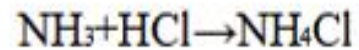
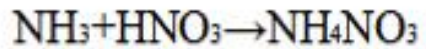
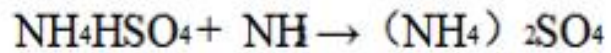
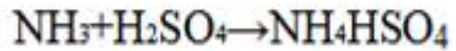
1. Ammonium salts such as ammonium nitrate and ammonium sulfate constitute an important fraction of the total fine particulate matter (PM_{2.5}) mass.
2. While the conversion of inorganic gases into particulate-phase sulfate, nitrate, and ammonium is now well understood, there is considerable uncertainty over interactions between gas-phase ammonia and secondary organic aerosols (SOAs).
3. Recently, chemical uptake coefficients for ammonia onto SOA were reported for the first time by Liu et al. (2015). Those coefficients were on the order of $\sim 10^{-3}$ – 10^{-2} for fresh SOA, decreasing significantly to $< 10^{-5}$ after 6 h of reaction.
4. In order to investigate the importance of such reactions, a first-order loss rate for ammonia onto SOA was implemented into the Community Multiscale Air Quality (CMAQ) model based on the ammonia uptake coefficients reported in the literature.



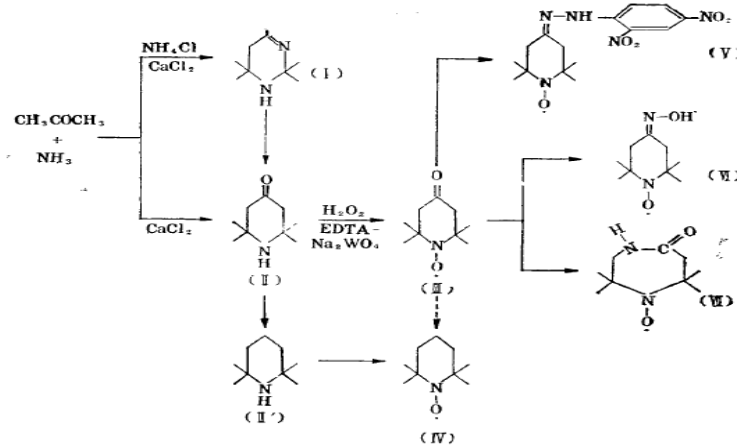
Introduction

Three reactions of ammonia in the atmosphere:

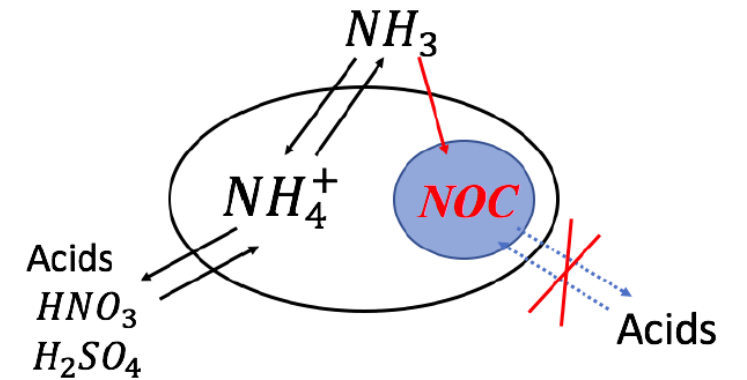
1. Neutralization of acids and bases in the atmosphere:



2. Reacting with free radicals and ozone in the atmosphere:



3. Atmospheric heterogeneous reaction:





Introduction

About WRF-CMAQ model:

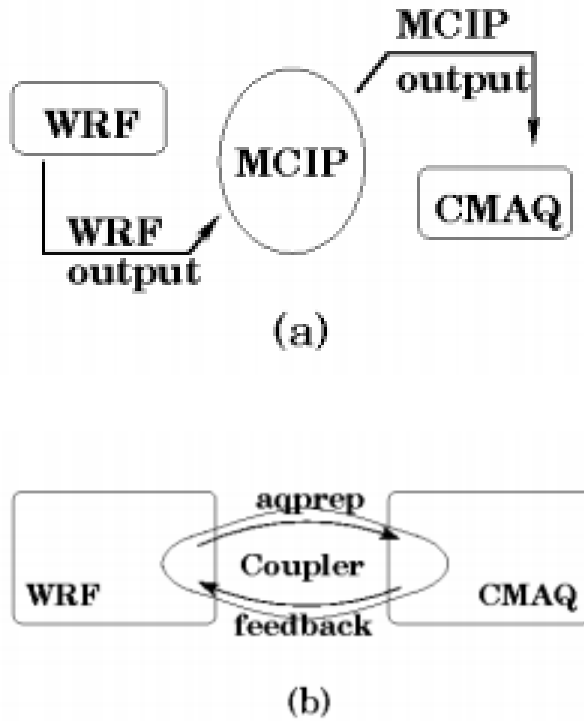
The Community Multiscale Air Quality (CMAQ) modeling system is being developed and maintained under the leadership of the EPA National Exposure Research Laboratory in Research Triangle Park, NC. CMAQ represents over two decades of research in atmospheric modeling and has been in active development since the early 1990's.

Under the authority of the Clean Air Act, the U.S. Environmental Protection Agency (EPA) has established National Ambient Air Quality Standards (NAAQS) (U.S. EPA, 2008). These standards are designed to protect human health and the environment from high levels of criteria pollutants, such as ozone and particulate matter. Meeting the NAAQS often requires the use of controls on sources of air pollutants. The complex nature of air pollution scenarios requires control strategies to be effective for a variety of air pollutants, geographic regions, and scales. As part of the effort to decrease ambient concentrations of criteria pollutants, the EPA has approved air quality simulation models for use at regional, state, and local scales within the United States. The models have been applied to estimate the ability of various control strategies to improve air quality and ensure cost-effective results.



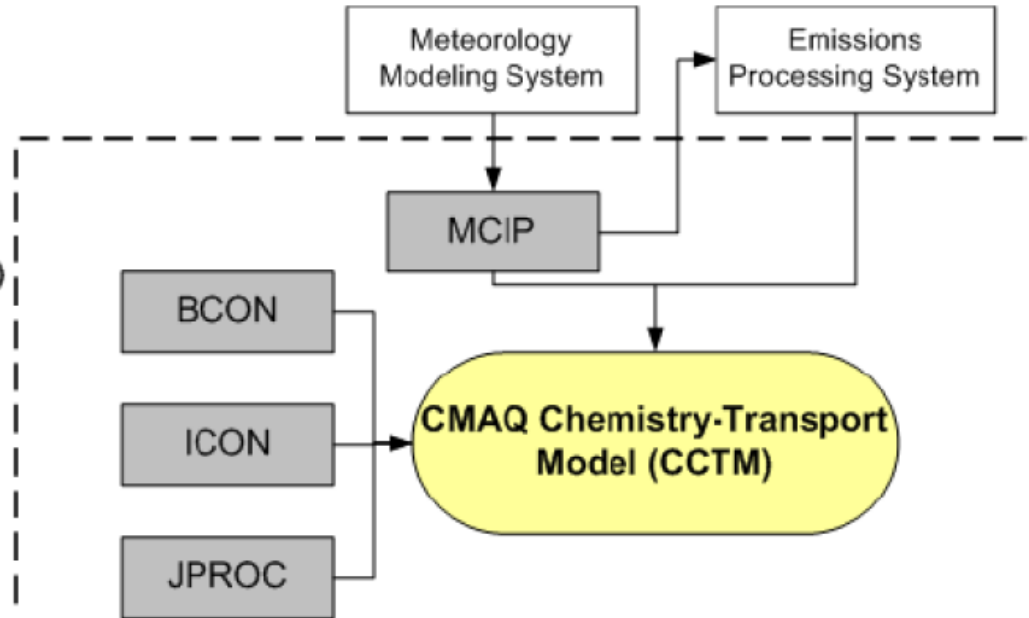
Introduction

About WRF-CMAQ model:



Options Selected

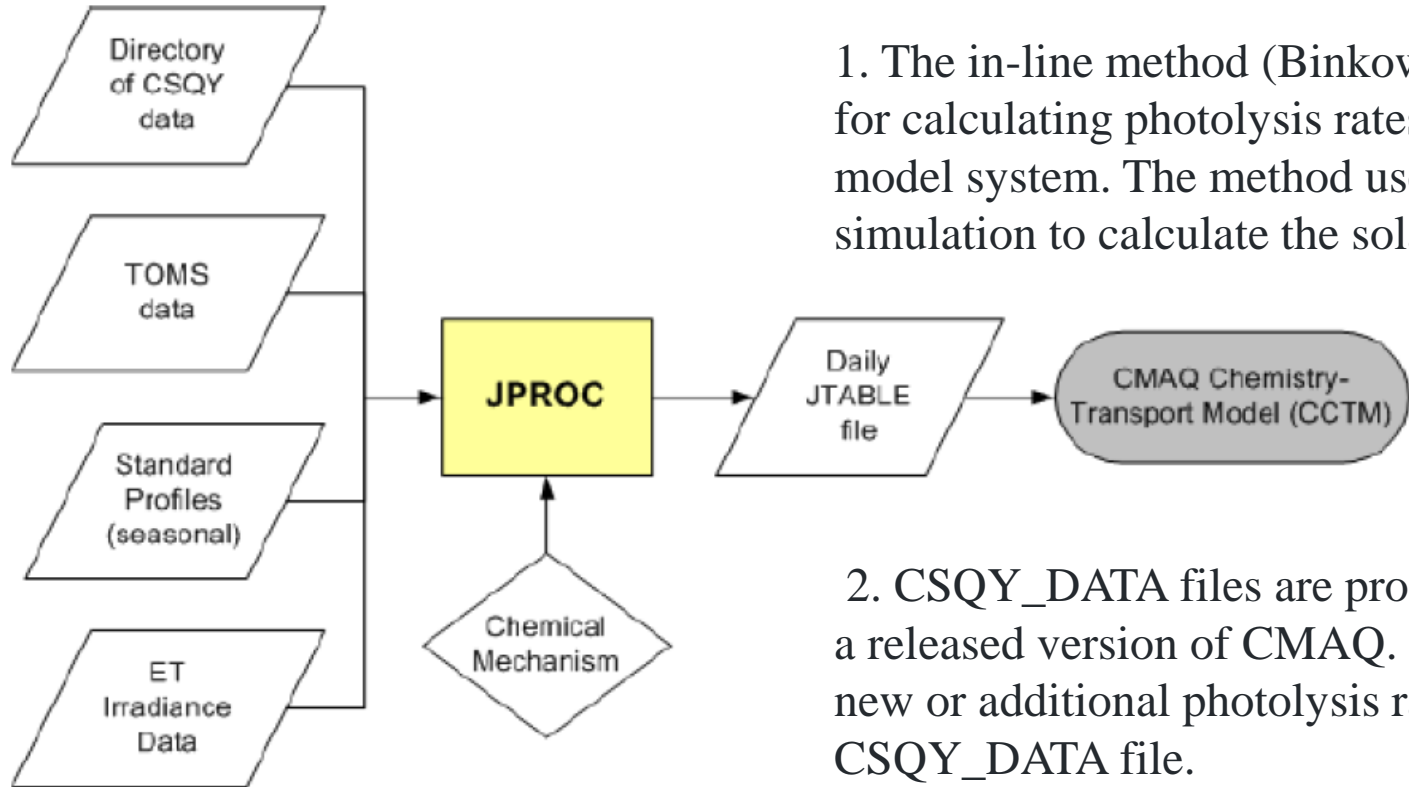
- Case
- Grid (Domain and Size)
- Projection
- Vertical Structure
- Chemical Mechanism





Introduction

About WRF-CMAQ model:



1. The in-line method (Binkowski et al., 2007) is the preferred method for calculating photolysis rates in the CCTM program of CMAQ model system. The method uses aerosol and ozone predicted within a simulation to calculate the solar radiation.

2. CSQY_DATA files are provided for all chemical mechanisms in a released version of CMAQ. If a user creates a mechanism using new or additional photolysis rates, they have to create a new CSQY_DATA file.



Introduction

About WRF-CMAQ model:

- SOA species in blue are semivolatile.
- SOA species in green are low volatility and treated as effectively nonvolatile.
- SOA species in yellow form due to reactive uptake and are treated as nonvolatile.
- SOA formed from particle-phase processing is in purple.

SOA species	version introduced	precursor	oxidants	semivolatile	alpha (mass-based)	C* (ug/m3)	enthalpy (kJ/mol)	number of C	molec wt (g/mol)	OM/OC	Model ref	Experimental ref
AALK1	v5.1	long-chain alkanes	OH	SV_ALK1	0.0334	0.1472	53.0	12	168	1.17	Pye and Pouliot 2012	Presto et al. 2010
AALK2	v5.1	long-chain alkanes	OH	SV_ALK2	0.2164	51.8774	53.0	12	168	1.17	Pye and Pouliot 2012	Presto et al. 2010
AXYL1	v4.7	XYL/ARO2 excluding naphthalene	OH,NO	SV_XYL1	0.0310	1.3140	32.0	8	192	2.0	Carlton et al. 2010	Ng et al. 2007
AXYL2	v4.7	XYL/ARO2 excluding naphthalene	OH,NO	SV_XYL2	0.0900	34.4830	32.0	8	192	2.0	Carlton et al. 2010	Ng et al. 2007
AXYL3	v4.7	XYL/ARO2 excluding naphthalene	OH,HO2	NA-nonvolatile	0.36	NA	NA	NA	192	2.0	Carlton et al. 2010	Ng et al. 2007
ATOL1	v4.7	TOL/ARO1	OH,NO	SV_TOL1	0.0310	2.3260	18.0	7	168	2.0	Carlton et al. 2010	Ng et al. 2007
ATOL2	v4.7	TOL/ARO1	OH,NO	SV_TOL2	0.0900	21.2770	18.0	7	168	2.0	Carlton et al. 2010	Ng et al. 2007
ATOL3	v4.7	TOL/ARO1	OH,HO2	NA-nonvolatile	0.30	NA	NA	NA	168	2.0	Carlton et al. 2010	Ng et al. 2007
ABNZ1	v4.7	benzene	OH,NO	SV_BNZ1	0.0720	0.3020	18	6	144	2.0	Carlton et al. 2010	Ng et al. 2007
ABNZ2	v4.7	benzene	OH,NO	SV_BNZ2	0.8880	111.1100	18	6	144	2.0	Carlton et al. 2010	Ng et al. 2007
ABNZ3	v4.7	benzene	OH,HO2	NA-nonvolatile	0.37	NA	NA	NA	144	2.0	Carlton et al. 2010	Ng et al. 2007
APAH1	v5.1	naphthalene	OH,NO	SV_PAH1	0.2100	1.6598	18	10	243	2.03	Pye et al. 2012	Chan et al. 2009
APAH2	v5.1	naphthalene	OH,NO	SV_PAH2	1.0700	264.6675	18	10	243	2.03	Pye et al. 2012	Chan et al. 2009
APAH3	v5.1	naphthalene	OH,HO2	NA-nonvolatile	0.73	NA	NA	NA	243	2.03	Pye 2012	Chan 2009
AISO1	v4.7	isoprene	OH,NO3	SV_ISO1	0.2320	116.010	40	5	96	1.6	Carlton et al. 2010	Kroll et al. 2006
AISO2	v4.7	isoprene	OH,NO3	SV_ISO2	0.0288	0.6170	40	5	96	1.6	Carlton et al. 2010	Kroll et al. 2006
AISO3	v5.1	IEPOX	NA-acid catalyzed uptake	NA-nonvolatile	NA	NA	NA	NA	168.2	2.7	Pye et al. 2013	Eddingsaas et al. 2010
ATRP1	v4.7	monoterpenes	OH,O3P,O3,NO3	SV_TRP1	0.1393	14.7920	40	10	168	1.4	Carlton et al. 2010	Griffin et al. 1999
ATRP2	v4.7	monoterpenes	OH,O3P,O3,NO3	SV_TRP2	0.4542	133.7297	40	10	168	1.4	Carlton et al. 2010	Griffin et al. 1999
ASQT	v4.7	sesquiterpenes	OH,O3,NO3	SV_SQT2	1.5370	24.9840	40	15	378	2.1	Carlton et al. 2010	Griffin et al. 1999
AOLGA	v4.7	anthropogenic SOA	time	NA-nonvolatile	NA	NA	NA	NA	176.4	2.1	Carlton et al. 2010	Kalberer et al. 2004
AOLGB	v4.7	biogenic SOA	time	NA-nonvolatile	NA	NA	NA	NA	252	2.1	Carlton et al. 2010	Kalberer et al. 2004
AORGC	v4.7	SOA from cloud processing of glyoxal, methylglyoxal	OH	NA-nonvolatile	NA	NA	NA	NA	177	2.0	Carlton et al. 2008	



Methods

Hypotheses

1. In this study, all NH_3 taken up by SOA carbonyls is assumed to form NOCs, such as secondary imines and heteroaromatic compounds

2. The difference in molecular weights of two H_2O molecules and one NH_3 molecule ($2 \times 18 - 17 = 19 \text{ g mol}^{-1}$) is small relative to a molecular weight of a typical SOA compound (about 200 g mol^{-1}). Therefore, for the sake of simplicity, we neglected the loss of the mass of particulate organics mass directly due to the NH_3 uptake in this simulation. This assumption is supported by experimental observations described by Horne et al. (2018), in which SOA particles exposed to ammonia in a smog chamber did not change their size distribution but showed clear evidence of incorporation of organic nitrogen into the particles in online and offline mass spectra.



Methods

In this study, the AERO6 module in CMAQ was updated to simulate the heterogeneous uptake of NH₃ by SOA.

$$S_{SOA} = \sum_{j=1}^x \left(S_j \times \frac{\sum_{i=1}^y m_{ij}}{\sum_{k=1}^z m_{kj}} \right)$$

In the AERO6 modal approach, three integral properties of the size distribution are followed for mode j : the total particle number concentration N_j , the total wet surface area concentration S_j , and the total mass concentration m_{ij} of each individual chemical component i . In order to calculate the total uptake of NH₃ by SOA, one must know the representative wet surface area concentration of SOA (S_{SOA}) (SOA hygroscopic growth is not considered in the model), which can be calculated as follows (assuming a uniform density across different chemical components):

$$k = \gamma \times \frac{v_{NH_3} \times S_{SOA}}{4}$$

where γ is the reactive uptake coefficient for ammonia and v_{NH_3} is the average speed of NH₃ molecules (609ms⁻¹ at 298 K). The above calculations were performed separately for each grid cell at every time step to obtain the effective first-order rate constant for each individual cell at each time step. The first-order rate constant of NH₃ uptake was then multiplied by the gas-phase NH₃ concentration to determine the loss rate of NH₃ in each cell at each time step.



Methods

Data information

1. base case simulation results of $PM_{2.5}$, PM_{10} , and O_3 are compared with the observations from the US Environmental Protection Agency's Air Quality System (AQS)
2. The meteorological fields were derived from NCEP FNL (Final) Operational Global Analysis data (NCEP, 2000) using the Weather Research and Forecasting Model (WRF, version 3.7) (Skamarock et al., 2008), with the MODIS land use database (Friedl et al., 2010) and the the Yonsei University (YSU) parametrization (Hong et al., 2006) for the planetary boundary layer.
3. Emissions were generated based on the 2014 National Emissions Inventory (NEI) (US EPA, 2017a) and processed by the Sparse Matrix Operator Kernel Emission (SMOKE , version 4.5) processor (US EPA, 2017b).
4. Biogenic emissions were obtained from the Biogenic Emission Inventory System (BEIS) (Pierce and Waldruff , 1991), and emissions from cars, trucks, and motorcycles were calculated with MOBILE6 (US EPA, 2003).



Methods

Modeling method

1. In this study, eight simulations were conducted using the latest 2017 release of **CMAQ** (version 5.2), including one base case simulation for the winter (**Jan. 1 - Feb. 27, 2011**), one base case simulation for the summer (**1 July–30 August 2011**), and three different NH_3 uptake scenarios for each period.
2. The modeling domain used in this study covers the contiguous US using a **12 km 12 km** horizontal-grid resolution (resulting in $396 (x) \times 246 (y) = 97\,416$ grid cells) and a **29-layer** logarithmic vertical structure (set on a terrain following sigma coordinate, **from the surface to 50 hPa**) with the depth of the first layer around 26 m.

Test method

1. four simulations were performed for each period to investigate the sensitivity of NH_3 removal to changes in the uptake coefficient: (a) base case with no NH_3 uptake, (b) NH_3 uptake with $\gamma=10^{-3}$, (c) NH_3 uptake with $\gamma=10^{-4}$, and (d) NH_3 uptake with $\gamma=10^{-5}$.
2. Results of the first 7 days of each simulations were discarded as a model spin-up period to minimize the effect of initial conditions and allow sufficient time for the NH_3 removal process to occur.



Results

Model validation

The statistical parameters used in this study are the mean normalized gross bias (MNGB), mean normalized gross error (MNGE), mean fractional bias (MFB), and mean fractional error (MFE).

($|MNGB| \leq 15\%$ and $MNGE \leq 30\%$)

($MFE \leq 75\%$ and $|MFB| \leq 60\%$)

Statistic indicator	Definition
Root mean square error (RMSE)	$\sqrt{\frac{1}{n} \sum_{i=1}^n (c_i - o_i)^2}$
Correlation	$\frac{\sum_{i=1}^n (c_i - \bar{c})(o_i - \bar{o})}{\sqrt{\sum_{i=1}^n (c_i - \bar{c})^2} \sqrt{\sum_{i=1}^n (o_i - \bar{o})^2}}$
Mean normalised gross bias (MNGB)	$\frac{1}{n} \sum_{i=1}^n \frac{o_i - c_i}{c_i}$
Mean normalised gross error (MNGE)	$\frac{1}{n} \sum_{i=1}^n \frac{ o_i - c_i }{c_i}$
Mean fractional bias (MFB)	$\frac{1}{n} \sum_{i=1}^n \frac{c_i - o_i}{(c_i + o_i)/2}$
Mean fractional error (MFE)	$\frac{1}{n} \sum_{i=1}^n \frac{ c_i - o_i }{(c_i + o_i)/2}$



Results

Model validation(O₃)

Period	Obs. mean ppb	Sim. mean ppb	RMSE ppb	Corr. %	MNGB %	MNGE %	No. sites
Summer	41.1	50.9	16.7	56.7	12.0	29.7	1262
Winter	27.3	33.9	10.4	51.4	8.8	23.1	664

shows good model performance for O₃, as the statistics meet the recommended performance criteria ($|MNGB| \leq 15\%$ and $MNGE \leq 30\%$)

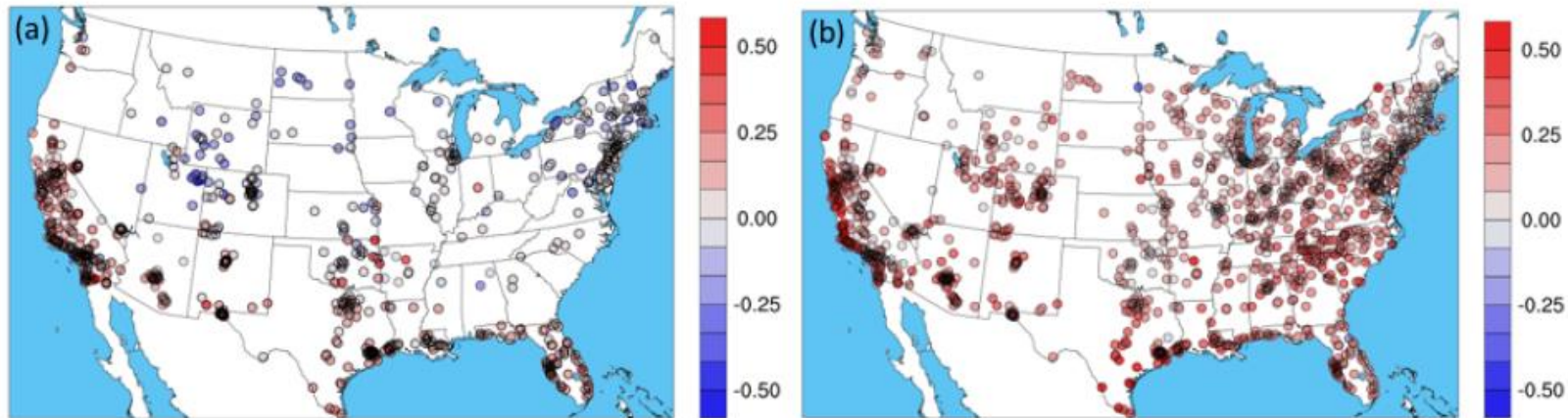


Figure S2. O₃ Mean Normalized Gross Bias at AQS sites for the base case CMAQ model simulation, (a) for winter period, (b) for summer period. Red values indicate an overestimation and blue values indicate an underestimation.



Results

Model validation($PM_{2.5}$)

Scenario	Period	Obs. mean $\mu\text{g m}^{-3}$	Sim. mean $\mu\text{g m}^{-3}$	RMSE $\mu\text{g m}^{-3}$	Corr. %	MFB %	MFE %	No. sites
Base	Summer	12.6	21.9	18.1	17.8	36.7	62.7	176
$\gamma = 10^{-3}$	Summer	12.6	24.1	20.5	18.3	41.2	66.3	176
$\gamma = 10^{-4}$	Summer	12.6	22.1	18.4	17.8	37.2	63.1	176
$\gamma = 10^{-5}$	Summer	12.6	21.9	18.1	17.8	37.0	62.9	176
Base	Winter	12.3	13.0	11.4	31.3	2.8	60.9	166
$\gamma = 10^{-3}$	Winter	12.3	12.6	11.1	31.4	0.6	60.4	166
$\gamma = 10^{-4}$	Winter	12.3	12.9	11.4	31.4	2.4	60.8	166
$\gamma = 10^{-5}$	Winter	12.3	13.0	11.4	31.3	2.7	60.9	166

For the winter, increasing the NH_3 uptake coefficient leads to a decrease in the total $PM_{2.5}$ and a slightly better model performance when compared to the observations.





Results

Model validation(NH₃)

Scenario	Period	Obs. mean $\mu\text{g m}^{-3}$	Sim. mean $\mu\text{g m}^{-3}$	RMSE $\mu\text{g m}^{-3}$	Corr. %	MFB %	MFE %	No. sites
Base	Summer	1.36	2.17	1.41	20.2	46.7	72.2	46
$\gamma = 10^{-3}$	Summer	1.36	0.63	1.07	-26.1	-70.1	96.4	46
$\gamma = 10^{-4}$	Summer	1.36	1.48	1.08	-2.0	7.3	63.2	46
$\gamma = 10^{-5}$	Summer	1.36	1.30	1.30	18.1	38.0	68.9	46
Base	Winter	0.77	0.37	0.57	26.2	-63.3	88.7	19
$\gamma = 10^{-3}$	Winter	0.77	0.31	0.60	29.7	-78.9	98.0	19
$\gamma = 10^{-4}$	Winter	0.77	0.36	0.58	27.5	-65.9	90.1	19
$\gamma = 10^{-5}$	Winter	0.77	0.37	0.57	26.5	-63.6	88.9	19

the model overestimates the NH₃ concentration for the summer, especially over the southeast and the Central Valley regions of California. On the contrary, the simulated NH₃ concentration is underestimated for the winter. The impacts of different NH₃ uptake coefficients on NH₃ concentrations are consistent between the winter and the summer; the NH₃ concentration decreases as the uptake coefficient increases.





Results

Model validation(NH_4^+)

Scenario	Period	Obs. mean $\mu\text{g m}^{-3}$	Sim. mean $\mu\text{g m}^{-3}$	RMSE $\mu\text{g m}^{-3}$	Corr. %	MFB %	MFE %	No. sites
Base	Summer	0.82	0.98	0.70	31.8	7.7	71.3	187
$\gamma = 10^{-3}$	Summer	0.82	0.83	0.62	31.4	-5.3	70.3	187
$\gamma = 10^{-4}$	Summer	0.82	0.92	0.66	32.0	3.2	70.5	187
$\gamma = 10^{-5}$	Summer	0.82	0.96	0.69	31.9	6.8	71.1	187
Base	Winter	1.30	1.20	0.96	45.8	-12.8	64.5	187
$\gamma = 10^{-3}$	Winter	1.30	1.08	0.93	45.1	-21.1	64.3	187
$\gamma = 10^{-4}$	Winter	1.30	1.18	0.95	45.6	-14.1	64.4	187
$\gamma = 10^{-5}$	Winter	1.30	1.20	0.96	45.8	-12.9	64.4	187

the NH_4 is slightly overestimated in the base case for the summer period; however, the addition of NH_3 uptake leads to a lower modeled NH_4 concentration and reduced level of overestimation. Such improvements happen over most of the eastern US as well as the Central Valley of California. Similar to NH_3 , the $\gamma=10^{-4}$ case shows better model performance improvement than the $\gamma=10^{-3}$ case in the summer. For the winter, the NH_4 concentration is slightly underestimated in the base case, so the decrease in the NH_4 concentration caused by the increase in the NH_3 uptake coefficient leads to an even larger underestimation.



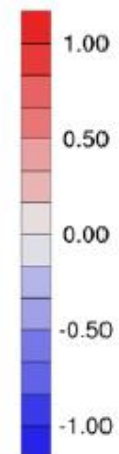
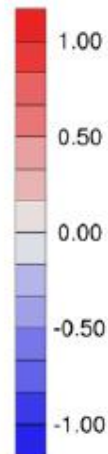


Results

Model validation(NO_3^-)

Scenario	Period	Obs. mean $\mu\text{g m}^{-3}$	Sim. mean $\mu\text{g m}^{-3}$	RMSE $\mu\text{g m}^{-3}$	Corr. %	MFB %	MFE %	No. sites
Base	Summer	0.47	0.88	0.85	17.8	31.1	87.3	187
$\gamma = 10^{-3}$	Summer	0.47	0.46	0.54	14.7	-38.2	90.1	187
$\gamma = 10^{-4}$	Summer	0.47	0.70	0.68	18.2	10.3	80.6	187
$\gamma = 10^{-5}$	Summer	0.47	0.84	0.81	18.1	27.6	85.8	187
Base	Winter	2.43	3.14	2.57	40.4	31.0	75.2	187
$\gamma = 10^{-3}$	Winter	2.43	2.74	2.29	40.0	20.5	71.0	187
$\gamma = 10^{-4}$	Winter	2.43	3.07	2.52	40.4	29.3	74.4	187
$\gamma = 10^{-5}$	Winter	2.43	3.13	2.56	40.4	30.8	75.1	187

the modeled NO_3^- is overestimated over the southeast region for both periods and also overestimated along the Central Valley of California during the summer period.





Results

Air quality impacts(gas-phase NH₃)

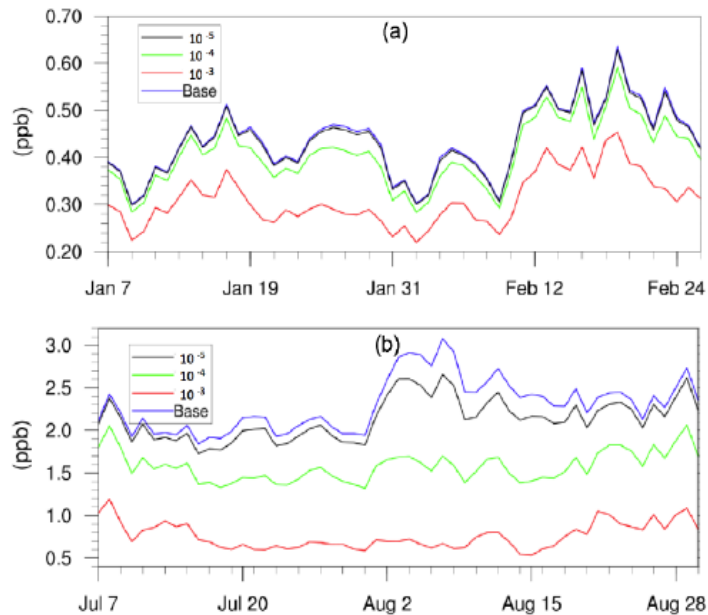


Figure S12. Daily, spatially-averaged NH₃ concentrations for different uptake coefficient scenarios for (a) winter period, and (b) summer period

In general, the NH₃ concentration is reduced after the introduction of the SOA-based NH₃ uptake process. The magnitude of the reduction is increased as the uptake coefficient increases. For the winter, the spatiotemporally averaged (averaged over entire period and the simulation domain) NH₃ concentration for the base case is 0.44 ppb, while the value decreases to 0.43 ppb (-2.3 %) for the $\gamma=10^{-5}$ case, 0.41 ppb (-6.8 %) for the $\gamma=10^{-4}$ case, and 0.31 ppb (-29.5 %) for $\gamma=10^{-3}$ case. For the summer, the spatiotemporally averaged NH₃ concentration for the base case is 2.30 ppb, while the value decreases to 2.10 ppb (-8.7 %) for $\gamma=10^{-5}$ case, 1.58 ppb (-31.3 %) for the $\gamma=10^{-4}$ case, and 0.76 ppb (-67.0 %) for the $\gamma=10^{-3}$ case.



Results

Air quality impacts(gas-phase NH_3)

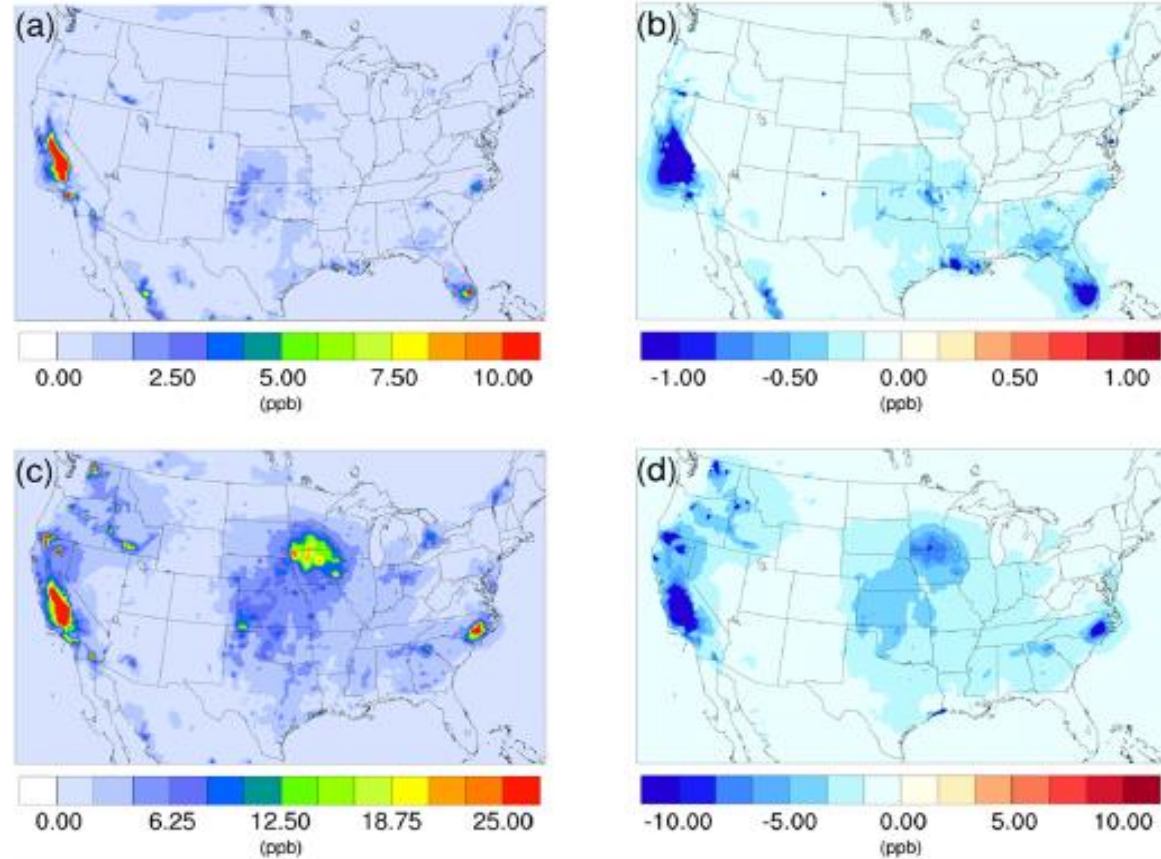


Figure 1. Spatial distribution of time-averaged NH_3 concentrations in the base case for (a) winter and (c) summer. Spatial distribution of the difference in time-averaged NH_3 concentrations between the $\gamma = 10^{-3}$ case and the base case for (b) winter and (d) summer. Negative values represent decreases in concentration with respect to the base case.



Results

Air quality impacts(gas-phase HNO_3)

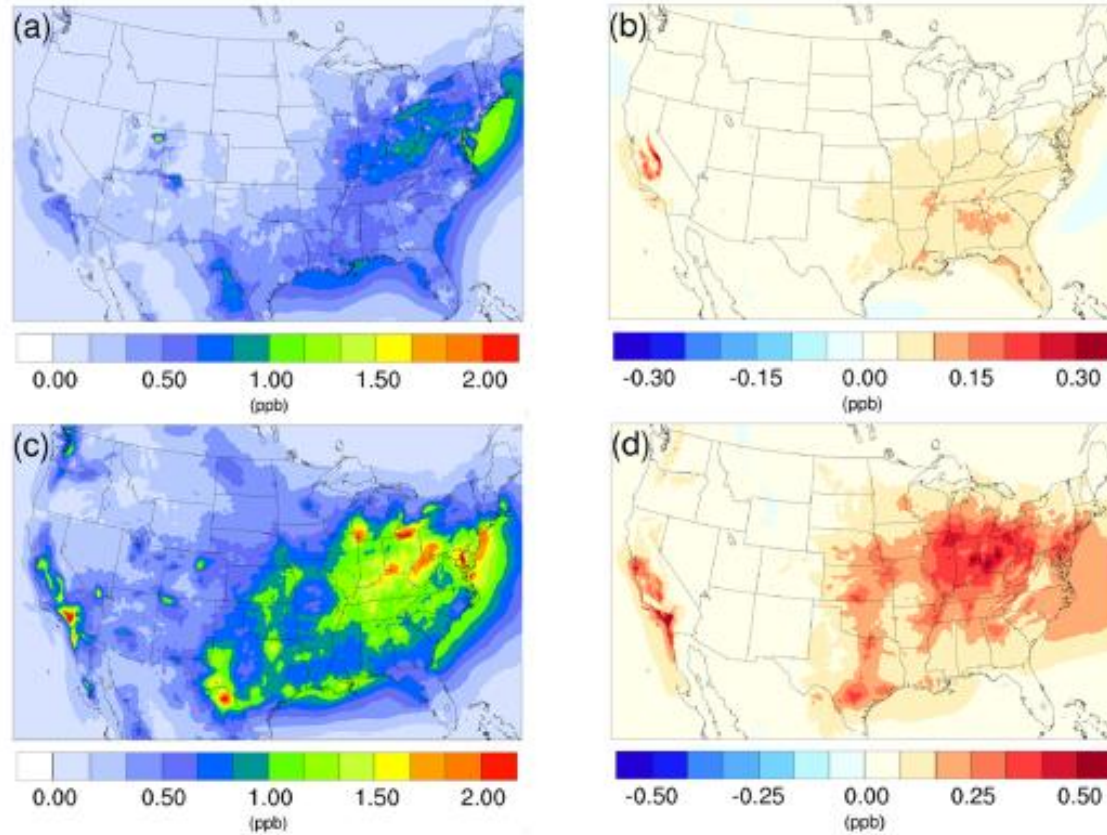


Figure 2. Spatial distribution of time-averaged HNO_3 concentrations in the base case for (a) winter and (c) summer. Spatial distribution of the difference in time-averaged HNO_3 concentrations between the $\gamma = 10^{-3}$ case and the base case for (b) winter and (d) summer. Positive values represent increases in concentration with respect to the base case.



Results

Air quality impacts (inorganic PM)

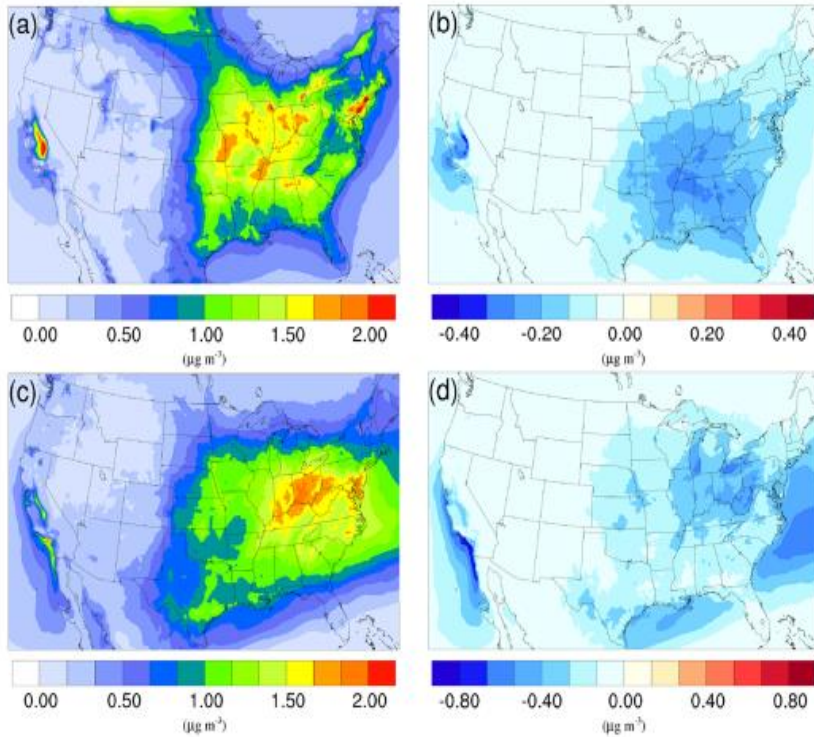


Figure 3. Spatial distribution of time-averaged NH_4^+ concentrations in the base case for (a) winter and (c) summer. Spatial distribution of the difference in time-averaged NH_4^+ concentrations between the $\gamma = 10^{-3}$ case and the base case for (b) winter and (d) summer. Negative values represent decreases in concentration with respect to the base case.

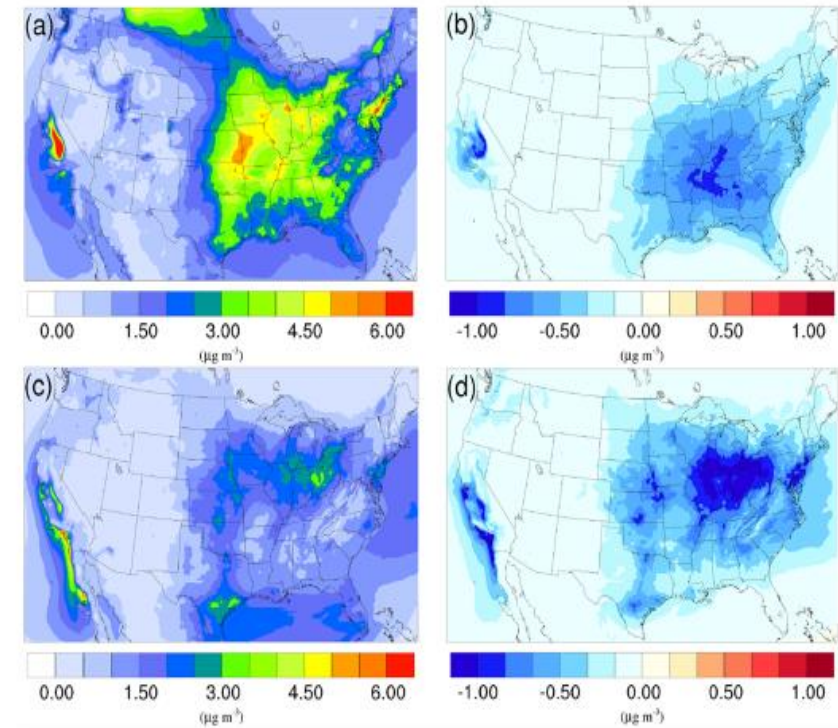


Figure 4. Spatial distribution of time-averaged NO_3^- concentrations in the base case for (a) winter and (c) summer. Spatial distribution of the difference in time-averaged NO_3^- concentrations between the $\gamma = 10^{-3}$ case and the base case for (b) winter and (d) summer. Negative values represent decreases in concentration with respect to the base case.



Results

Air quality impacts(organic PM)

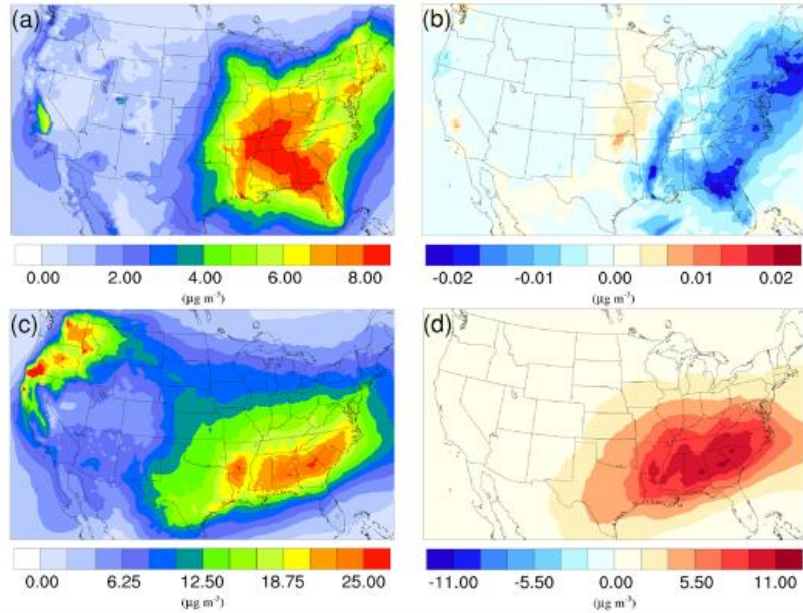


Figure 6. Spatial distribution of time-averaged SOA concentrations in the base case for (a) winter and (c) summer. Spatial distribution of the difference in time-averaged SOA concentrations between the $\gamma = 10^{-3}$ case and the base case for (b) winter and (d) summer. Positive values represent increases in concentration with respect to the base case, and negative values represent decreases in concentration with respect to the base case.

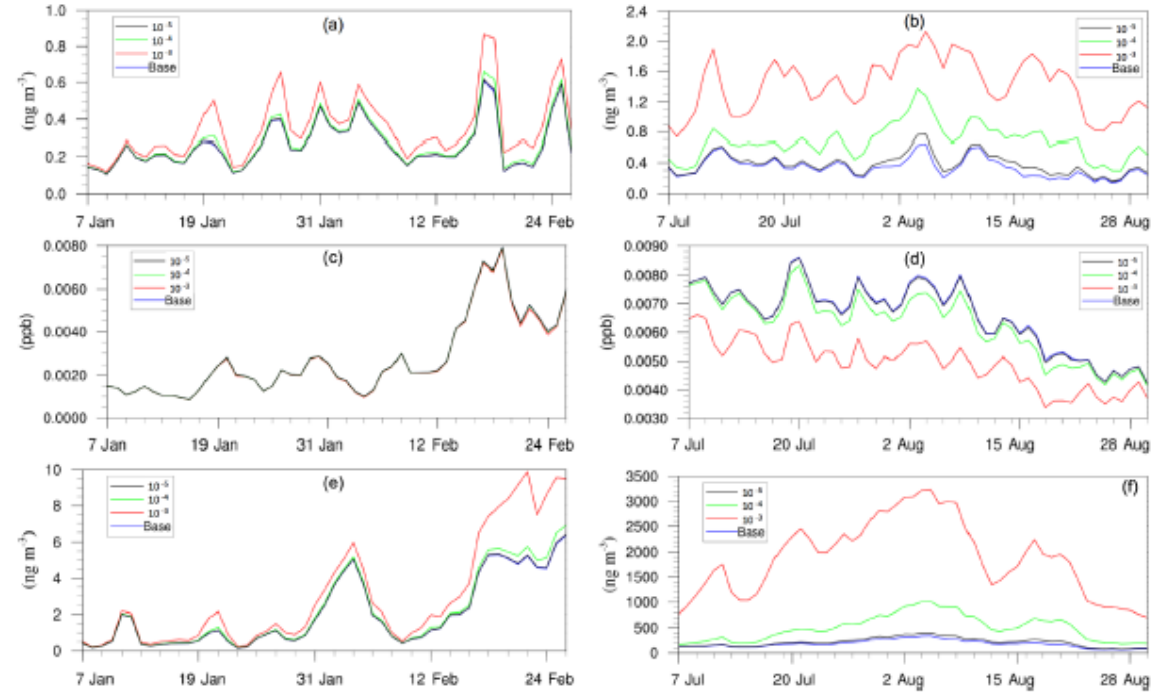
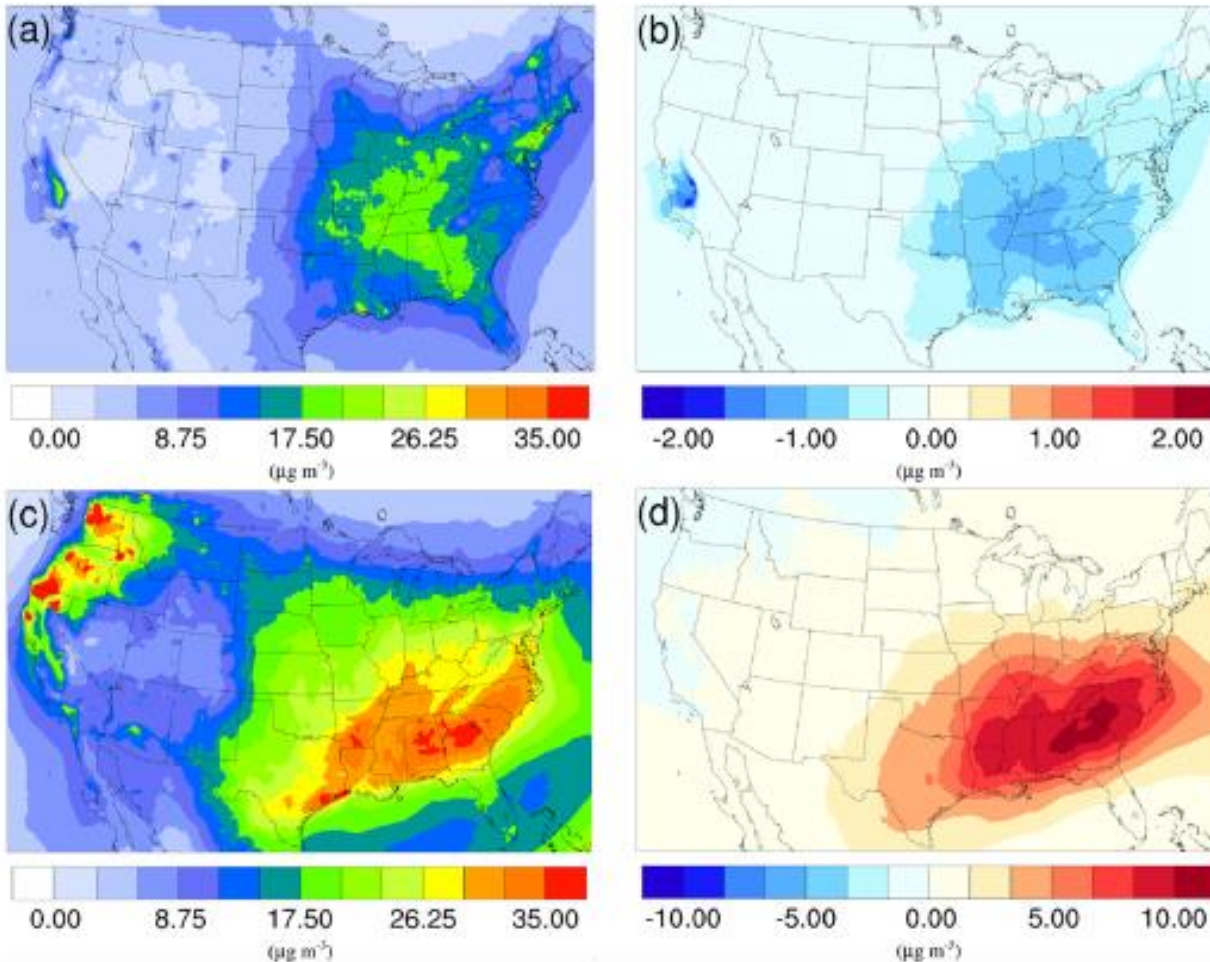


Figure 8. Daily, spatially averaged concentrations of (a) particle-phase H^+ in winter, (b) particle-phase H^+ in summer, (c) isoprene epoxydiols in winter, (d) isoprene epoxydiols in summer, (e) isoprene-epoxydiol-derived SOA in winter, and (f) isoprene-epoxydiol-derived SOA in summer.



Results

Air quality impacts(total PM)



1. both the pattern and level of impact caused by the NH_3 uptake mechanism is similar for $\text{PM}_{2.5}$ and PM_{10} , which indicates that most of the mass change due to this process occurs on fine particles.

2. the level of impact on both $\text{PM}_{2.5}$ and PM_{10} is much more significant over the summer than the winter, which is consistent with previous analysis of individual species.

3. Opposite impact patterns are found between the winter and summer. The inclusion of the NH_3 uptake mechanism leads to a decrease in the total PM mass for the winter, which is caused by the reduction of inorganic NH_4^+ and NO_3^- due to the decreasing the NH_3 concentration. On the contrary, PM concentrations during the summer increase after adding the NH_3 uptake mechanism.



Discussion

Conclusions

1. the simulation results for the two base case simulations are compared with observation data from different monitoring networks, and statistics show an overall good model performance for most of the criteria.

2. The comparison between different uptake coefficient scenarios and the base case allows a more detailed understanding of the impact of this mechanism on both gas-phase and particle-phase species.

2.1 Simulation results indicate a significant reduction in gas-phase NH_3 due to conversion of NH_3 into NOCs, and such reduction increases dramatically as the uptake coefficient increases

2.2 As the NH_3 concentration drops because it is being converted into NOCs, less HNO_3 is neutralized by NH_3 , resulting in an overall increase in HNO_3 concentration.

3. PM concentrations are found to decrease during the winter period, largely due to the reduction in ammonium nitrate formation caused by the decrease in gas-phase ammonia.



Results

Conclusions

4. PM concentrations are found to increase during the summer due to the increase in biogenic SOA production resulting from the enhanced acid-catalyzed ring-opening reactions.
5. Geographically, the biggest reduction in NH_3 happens in the Central Valley of California during both seasons, the same location as the biggest increase in HNO_3 in the winter. While for the summer, HNO_3 increases more dramatically over the South Coast Air Basin of California and the northeast region of the country.



Results

Inspirations and further work

1. Using related data of China for **verification**
2. Refine the SOA category and then simulate it and compare it
3. The same approach is used to simulate the response of SOA and other inorganic gases



Results

Thank you